Applied Physics A (2023) 129:802
https://doi.org/10.1007/s00339-023-07095-x

Applied Physics A
Materials Science & Processing

Tunable quintet ultra-narrowband metamaterial absorber based on Pi-inverted-Pi structures

Sare Nur Çuhadar[1] · Habibe Durmaz[1]

Received: 4 April 2023 / Accepted: 23 October 2023 / Published online: 28 October 2023

Abstract
In this article, a metamaterial multi-band perfect absorber with a Pi-inverted-Pi resonator is designed and investigated. It is observed that the meta-surface with a typical metal–insulator-metal structure showed nearly perfect absorption in almost five narrow bands with the lowest 93.6% and the highest 99.7% absorption level, according to the full-wave simulation results. The tunability of the Pi-inverted-Pi resonator has been examined based on the geometrical parameters. The origin of the five resonance bands has been analyzed based on the electric field and charge distributions occurring at the metal–dielectric interface. These resonance peaks are located at 1817.52 nm, 1968.38 nm, 2721.31 nm, 3765.6 nm, and 5740.63 nm wavelengths. The polarization dependence of the structure is investigated under TE and TM light, and our findings reveal that the Pi-inverted-Pi structure is partially polarization-dependent, which is a beneficial property for optical filtering. Compared to similar multi-band absorbers in the literature to the best of our knowledge, our proposed system offers a narrow band with high Q-factors of 118.7, 53, 32, 33, and 32 at each resonance wavelength. Therefore, our proposed design can be used in optical filters, Raman spectroscopy, bio-sensing, and many other applications, especially for the mid-infrared region's spectroscopic sensing and filtering applications.

Keywords Metamaterial absorber · Quintet-band absorber · Optical filters · Ultra-narrow band absorber · Plasmonic absorber

1 Introduction

Metamaterials, also known as artificially manufactured materials, have attracted great attention in the last decades with unique properties that are not available in nature [1]. Since the impedance of metamaterials ($z = \sqrt{\mu/\epsilon} = 1$) can be simply adapted to the surrounding media, by satisfying maximum power transfer from the incoming light into surface plasmon. Therefore near-perfect absorption of light can be achieved. Metal-based plasmonic metamaterials have attracted a lot of attention in recent years, such as biosensing [2], negative refractive index [3], stealth technologies [4], and optical filtering [5]. These plasmonic structures have a unique ability to manipulate light by releasing an electromagnetic wave oscillation along with the metal–insulator interface by the interaction of the electromagnetic field and free electrons between the same interface [6]. These properties yield Metal–Insulator–Metal (MIM) structures to get great attention in many research areas, and the potential of light control in nanoscale dimensions has been demonstrated with different applications based on single [7], double [8], and multiple-band MIMs [9]. However, single-band absorbers are disadvantageous in the sensitivity and detection of different spectral fingerprints in imaging, filtering, and spectroscopic applications [10]. To overcome these disadvantages, many researchers have recently focused on high-performance dual or multi-band absorbers [11].

In recent studies, plasmonic filters, including low-pass [12], high-pass [13], band-pass [14], or band-stop filter [15] structures, have been investigated. In previous studies, aperture- and temporal-coupling mechanisms are most commonly used in plasmonic absorber designs. However, the static tunability of aperture-based absorbers is challenging due to tuning the gap length and tuning to different output waveguides at resonant wavelengths [16]. Particle or resonator-based absorbers are preferred for spectroscopic detection and filtering with their simple structure than the cavity

✉ Habibe Durmaz
hdurmaz@kmu.edu.tr

1 Department of Electrical-Engineering, Karamanoglu Mehmetbey University, Karaman 70100, Türkiye

and waveguide structures with more challenging dimensions control.

In this study, a narrowband metamaterial absorber (MA) with nearly perfect absorption at five different wavelengths is designed in the mid-IR region. The MA under study consists of a thick Au optical mirror, SiO_2 dielectric material, and a Pi-Inverted Pi-shaped Au resonator on top. Pi-Inverted-Pi resonators are geometrically optimized to get a nearly perfect absorption at five resonance peaks associated with each part of the Pi-Inverted-Pi antenna structure. The electric field and charge distributions of the antennas at resonance wavelengths are also investigated. The relations between the charge distribution and the electric field are evaluated numerically. In addition, the TE and TM polarization performance of the MA is examined, and its polarization dependence is shown. The Q-factor of the designed MA structure is calculated, and a high Q factor (118.61) is obtained. Our designed MA system with its simple structure, simultaneous perfect absorption at five bands, and high-Q factor can be used in many potential applications, such as absorption filtering, spectroscopic sensing, and narrowband photodetector.

2 Material and methods

2.1 Numerical analysis

A schematic view of the proposed quintet-band MA is shown in Fig. 1a. The unit cell of MA structure consists of 120 nm SiO_2 dielectric layer sandwiched between 200 nm Au layer and 60 nm thick Au Pi-inverted-Pi shaped resonators. The bottom Au layer serves as an optical mirror to minimize the leakage of the incoming wave. The geometrical parameters of the MA platform are as follows: H and L represent the horizontal and vertical lengths of the big Pi-structure, while K and M indicate the horizontal and vertical lengths of the small Pi-structure. The absorption strength can be improved slightly for an optimized value of w for small and big Pi, individually. The width (w) of the structure is set to 140 nm for simplicity.

The spectral response of the proposed MA has been numerically studied by the Finite Difference Time Domain (FDTD) method by the Lumerical program. In numerical calculations, the Palik reference was used for Au and SiO_2 dielectric constants [17]. In the simulation, a single unit cell consisting of two different elements of big and small Pi-shaped antenna has been computed with periodic boundary conditions in x- and y-directions, and a perfectly matched layer is chosen for the z-direction. A plane wave light source is set along the z-direction.

The calculated absorption spectra of the designed MA have five narrow resonance bands at peak positions of $\lambda_1 = 1817.52$ nm, $\lambda_2 = 1968.38$ nm, $\lambda_3 = 2721.31$ nm, $\lambda_4 = 3765.6$ nm, and $\lambda_5 = 5740.63$ nm as depicted in Fig. 1b. The absorption strengths for the associated resonance wavelengths are 96% (at λ_1), 97.15% (at λ_2), 94.5% (at λ_3), 99.7% (at λ_4), and 93.6% (at λ_5). The full-width at half maximum (FWHM) and the quality factors ($\frac{\lambda_0}{\mathrm{FWHM}}$) of individual peaks are 15, 37, 85, 114, and 179; 118.7, 53, 32, 33, and 32, respectively. The narrower the peak, the higher the quality factor Q; therefore, it offers better optical performance. The designed MA structure has nearly perfect absorption in almost all five resonances and high Q-factor than those

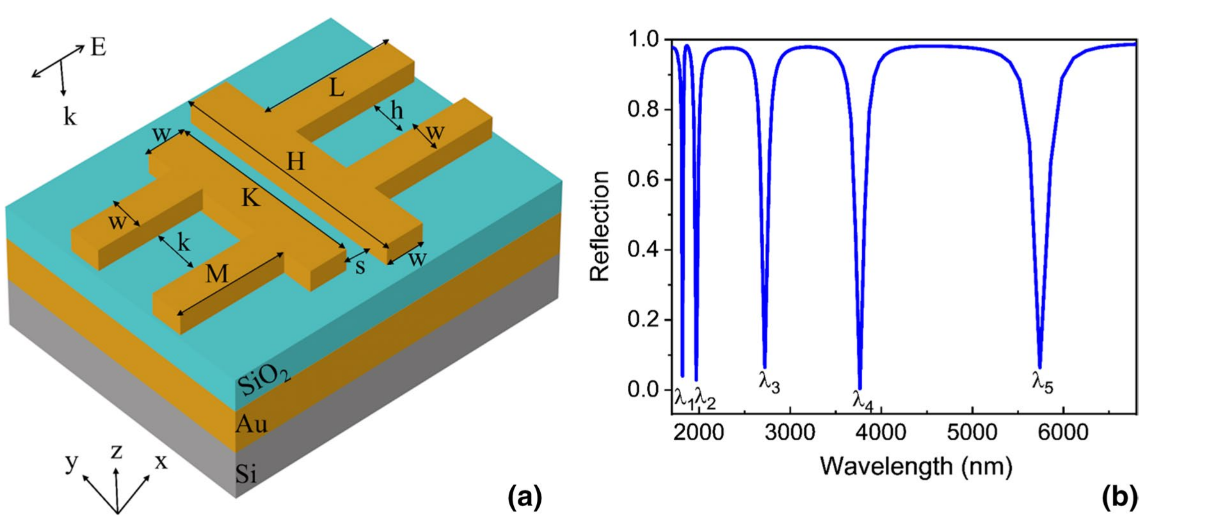

Fig. 1 **a** Schematic of the quintet band metamaterial absorber. **b** Calculated absorption spectrum with 200 nm thick Au layer as an optical mirror, 120 nm thick SiO_2 dielectric layer, and 60 nm thick Au resonators. The parameters of the part of the inverted-Pi-shaped antennas are $H = 1000$ nm, $L = 655$ nm, $M = 400$ nm, $K = 700$ nm, and $w = 140$ nm, respectively. The periodicity of the antennas is 1750 nm

reported in Table 1. These results reported in the table are obtained in a near-IR regime from 640 to 1644 nm, and the highest *Q*-factor is 87.6, which is almost two orders of magnitude small than our structure. In the longer wavelength regime, the FWHM increases due to the broadening of the bands; therefore, our structure has the highest *Q*-factor among its counterparts to the best of our knowledge.

The tuning capacity of the proposed MA has been investigated with the same FDTD method. It has been shown that the resonance peaks can be tuned spectrally depending on the geometric parameters (H, L, K, M, and P), as shown in Fig. 2. The change in the length (H) of the big Pi-antenna affects the spectral positions of the three resonances at λ_1, λ_3, and λ_5. The spectral shift for resonance at λ_1 has almost no change; however, absorption strength has significantly decreased as the H value changes from 1000 to 1300 nm. The spectral positions and the absorption strength of the resonances at λ_2 and λ_4 have no change at all. The spectral positions are the same for the value of 1100 nm and 1200 nm for the *H*-value at λ_5 with a strong decrease for $H = 1100$ nm. As the L parameter increases, the resonance wavelengths of λ_3 and λ_5 are red-shifted while the spectral positions at other resonances remain fixed, as shown in Fig. 2b. The near-unity perfect absorption can also be achieved at λ_1 (only for $L = 595$ nm), λ_4 (for all parameters), and λ_5 (only for $L = 545$ nm).

The resonance wavelength at λ_3 and λ_5 has no shift, while the other resonance has slight changes as the length *K* (varying between 580 and 760 nm) and *M* (ranging between 300 and 460 nm) as depicted in Fig. 2c and d. Also, the absorption strength is stable at λ_3, λ_4, and λ_5 with a change in the *K* value. The absorption strength decreases as *M* increases with a redshift. Also, the spectral tunability of resonance at λ_3 strongly depends on the *M* parameter. Figure 2e shows almost no effect of the period on the spectral position of the quintet resonances except at λ_5. These results show that the proposed structure is beneficial for frequency selective absorber applications with its single layer, easily controllable spectral positions, and simple structure.

The spectral response of the quintet absorber is almost stable with changing parameters of *h*, *s*, and *k* as shown in Fig. SI (1). This structure can be easily fabricated since the little variations in between the legs of each Pi and the gap between the Pi antennas has almost no effect on the spectral positions at five individual bands. Also, absorption strength does not change significantly at λ_1, λ_2, λ_3, and λ_4; however, at λ_5 it decreases to half.

Table 1 Comparison of our metamaterial absorber performance with the reported studies so far

References	Functionality	Resonance peak (nm)	Efficiency (%)	Q-factor	Publication year
[18]	Band-pass	732	70	36.27	2018
		1174	37	26.36	
[19]	Band-pass	640	44	12.9	2019
		1001	51	9.2	
[20]	Band-pass	1305	75	16.03	2013
		1613	82	10.75	
[16]	Band-pass	960	66	Not defined	2019
		1310	68		
[21]	Band-pass	1267.50	68.5	26.04	2020
		1414.19	78.6	15.88	
		1644.70	78.1	17.01	
[11]	Band-pass	876	97.6	87.6	2020
		998	99.3	66.5	
		1166	94.9	53	
		1411	88.7	40.3	
		1800	82.3	32.1	
[22]	Band-pass	1128	73	Not defined	2021
		1248	36		
		1362	43		
[This work]	Band-pass	1817.52	96.03	118.61	2022
		1968.38	97.15	52.73	
		2721.31	93.54	32.06	
		3765.60	99.66	32.92	
		5740.63	93.60	32.05	

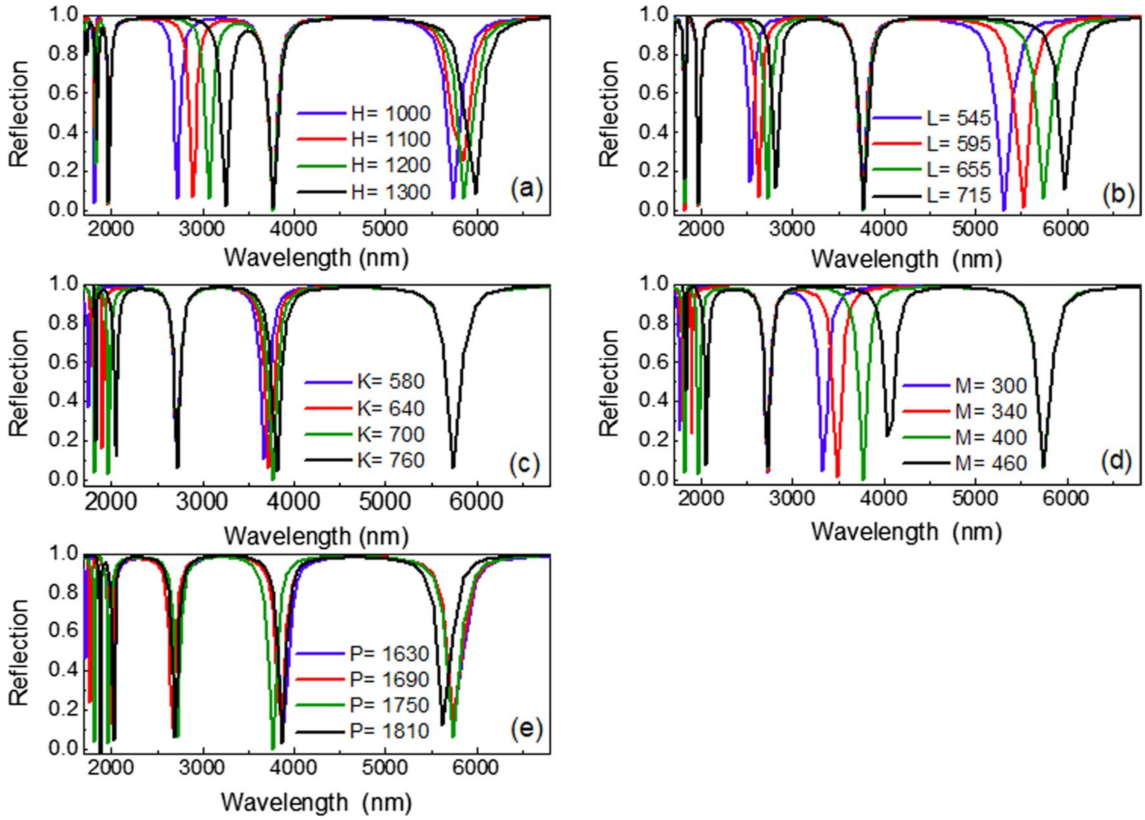

Fig. 2 The calculated absorption spectra of Pi-inverted-Pi-shaped metamaterial absorber. Spectral tuning based on geometrical parameters are given. **a** H parameter varies at fixed parameters of $L=655$ nm, $K=700$ nm, and $M=400$ nm. **b** L parameter varies at fixed parameters of $H=1000$ nm, $K=700$ nm, and $M=400$ nm. **c** K parameter varies at fixed parameters of $H=1000$ nm, $L=655$ nm, and $M=400$ nm. **d** M parameter varies at fixed $H=1000$ nm, $K=700$ nm, and $L=655$ nm. **e** The period varies at fixed parameters of $H=1000$ nm, $K=700$ nm, $L=655$ nm, and $M=400$ nm. The period is set as 1750 nm for **a**, **b**, **c**, and **d** for calculating the effect of other parameters

2.2 Field enhancements

In order to understand the physical origin of quintet resonance behavior, the field and charge distributions have been studied with the same FDTD method. Figure 3 shows the electric field intensity distributions at resonance wavelength at λ_1, λ_2, λ_3, $\lambda_{4,}$ and λ_5 in the metal layers. Figure 3a shows the electric field intensity of the five resonance values. Based on the electric field enhancements in Fig. 3b, the resonances at $\lambda_1 = 1817.52$ nm is due to the coupling of small Pi and the legs (L) of the big Pi antennas. The resonance at $\lambda_2 = 1968.38$ nm is completely due to the K length of the small Pi antennas as depicted in Fig. 3c. The field enhancement shows that the resonance at $\lambda_3 = 2721.31$ nm is due to the big Pi antenna (H and L parameter), as shown in Fig. 3d. From the field distributions, the resonance at $\lambda_4 = 3765.6$ nm is due to the small Pi antenna (K and mostly M parameter). From Fig. 3f, the E-field is mostly localized in the legs (L) of the big-Pi antennas; therefore, the resonance at $\lambda_5 = 5740.63$ nm is due to the big-Pi antenna.

2.3 Charge distributions

In order to fully understand the physical origin of electric and magnetic resonance occurring in Pi-inverted-Pi-shaped antennas, the charge distributions of five nearly perfect resonance peaks are investigated by the FDTD method. Figure 4a shows the charge distributions of resonance peaks at λ_1, λ_2, λ_3, $\lambda_{4,}$ and λ_5 in the resonator. It can be seen from the same figure that equal sizes of different charge polarities are accumulated at the opposite side of the Pi-inverted-Pi antennas, indicating that the electric dipole is excited. The electromagnetic dipole of the structure at each resonant wavelength is excited by a strong electric field at both Pi structures. Figure 4b shows the charge distribution at the first resonance wavelength of 1817.52 nm. The charges of different polarities are accumulated at the end of the base and the tip of the legs of the small Pi antenna. In the same figure, the charges with opposite signs are accumulated left and right legs with the same polarity of the charges in the big Pi-antennas indicating that electric dipoles excitations. Also, the charge accumulation at the base of big P-antennas (a negative and

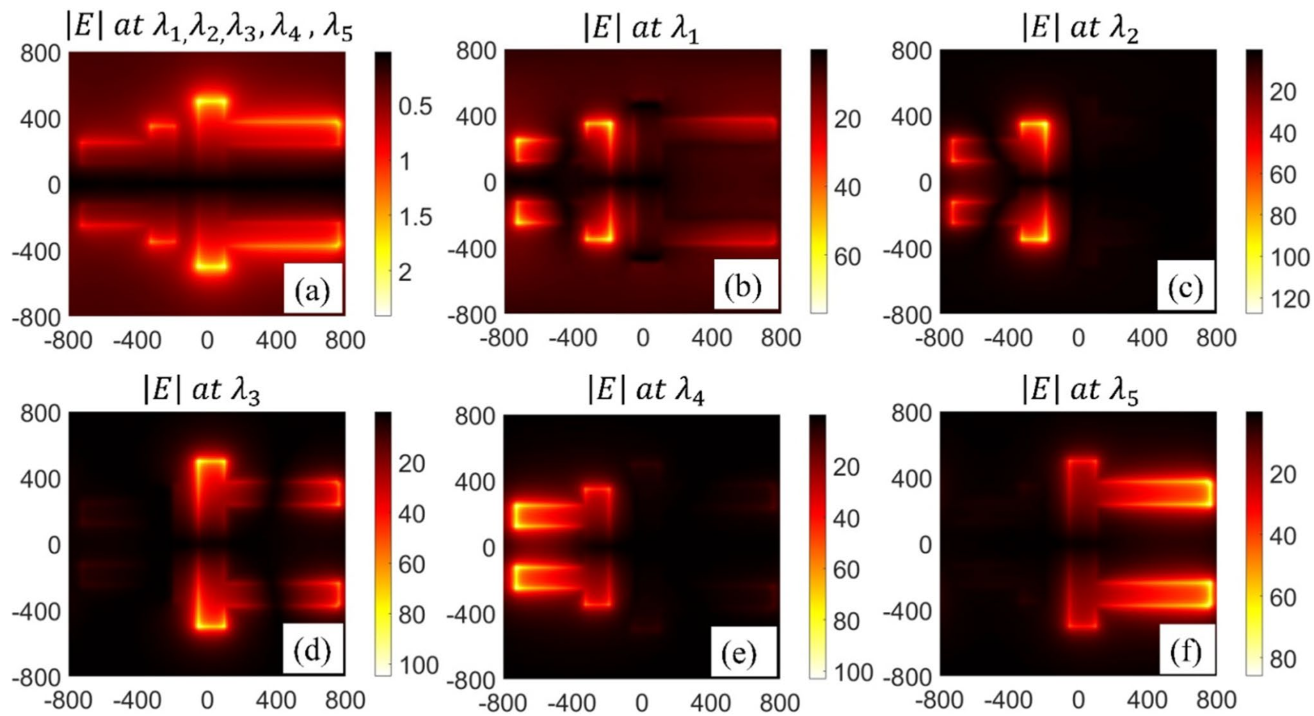

Fig. 3 Field enhancements at the interface between the dielectric layer and top metallic antennas for the proposed five-band Pi-inverted-Pi-shaped nano-antennas. The geometric parameters are $H=1000$ nm, $L=655$ nm, $K=700$ nm, $w=140$ nm, $M=400$ nm, and $s=140$ nm. The field enhancements of **a** all resonances, **b** resonance at λ_1, **c** the resonance at λ_2, **d** the resonance at λ_3, **e** the resonance at λ_4, and **f** the resonance at λ_5

positive charge) at the left and right parts, respectively, is mainly due to the coupling of the adjacent cell. The charge distributions at λ_2 (1968.38 nm) and λ_3 (2721.31 nm) indicate the excitation of two dipoles at the small and big Pi-antennas, respectively, as shown in Fig. 4c and d. The two poles of excited dipoles can be seen in the charge distributions at the resonance wavelengths of λ_4 (3765.6 nm) and λ_5 (5740.63 nm) in Fig. 4e and f, respectively. These charge accumulations given in Fig. 4 indicate the electric dipole excitations supported by the electric field enhancement due to surface plasmons.

2.4 Polarization dependence of the metamaterial absorber

Polarization sensitivity analysis is carried out to justify the choice of design structure. For TM polarization (90° polarization angle), the structure offers five absorption bands at 1817.52 nm, 1968.38 nm, 2721.31 nm, 3765.60 nm, and 5740.63 nm with the absorption level of 96.03%, 97.15%, 93.54%, 99.66%, and 93.60%, respectively. The structure is partially sensitive to polarization with 60%, 58%, and 50% absorption at 1817.52 nm, 1968.38 nm, and 50% at 2721.31 nm, respectively for TE polarization (0° polarization angle), as shown in Fig. 5. The peaks at 3765.6 nm and 5740.63 nm are disappeared for TE polarization. The structure was partially sensitive to polarization due to its asymmetrical design. The important design contribution of this work is that a single layer MA offers five and three significant absorption bands for TM and TE polarization, respectively. The proposed quintet band MA has potential applications in Mid-IR spectroscopy, bandpass filters, and optical filtering, etc.

3 Conclusion

In summary, a quintet-band metamaterial absorber based on Pi-inverted-Pi-shaped nano-antennas is proposed, and the absorption characteristics of the structure are numerically analyzed. The numerical results show that the absorption spectra of the proposed structure have five absorption bands at 1817.52 nm, 1968.38 nm, 2721.31 nm, 3765.6 nm, and 5740.63 nm. Near-perfect absorption is achieved at almost each of the five resonance wavelengths, simultaneously. Our numerical analyzes demonstrate that the origin of five resonances is due to the field coupling in the Pi-inverted-Pi-shaped antenna. The results also show that by changing the dimensions of the Pi-type resonator, the spectral position, number of peaks, and absorption strength of the five

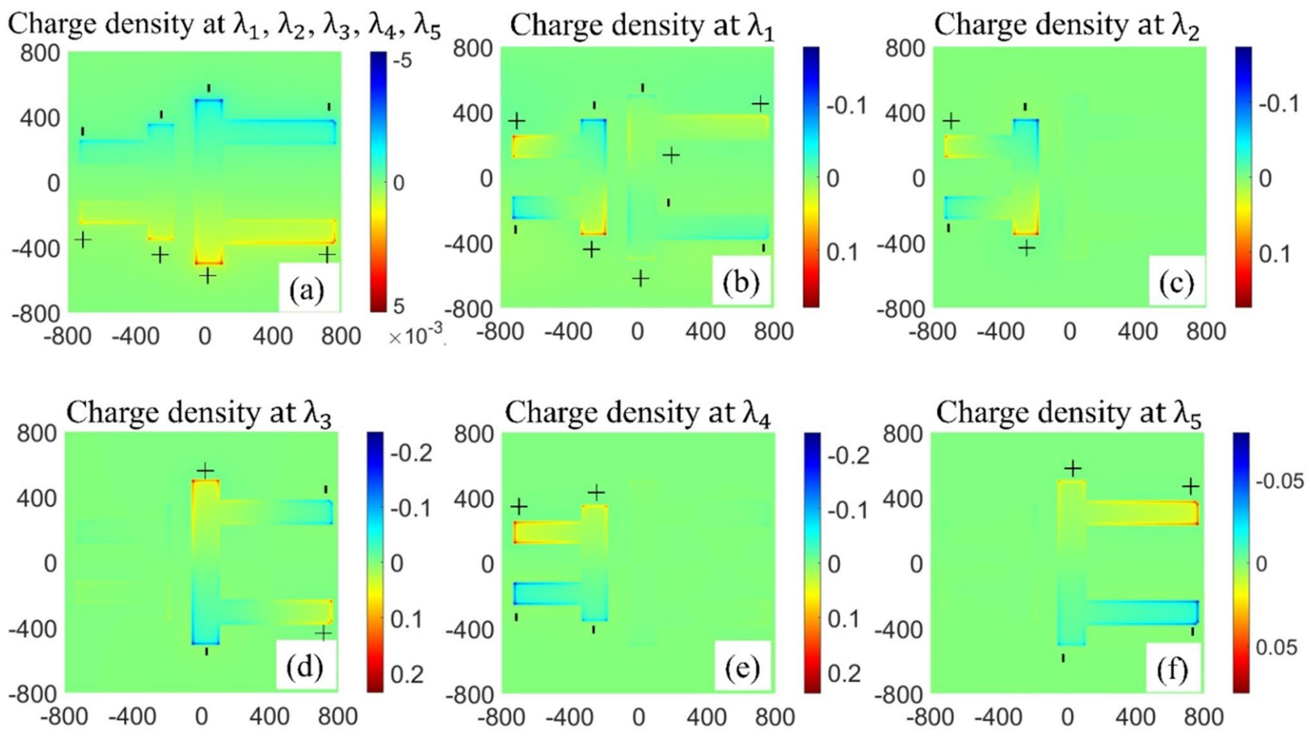

Fig. 4 Charge distributions of Pi-inverted-Pi-shaped nano-antennas. The geometric parameters $H = 1000$ nm, $L = 655$ nm, $K = 700$ nm, $M = 400$ nm, $w = 140$ nm, and $s = 140$ nm are used for calculations. **a** The charge distributions of all resonances. **b** The charge distribution at λ_1 resonance. **c** The charge distribution of resonance at λ_2. **d** The charge distribution of the λ_3 resonance. **e** The charge distribution at λ_4 resonance. **f** The charge distribution at λ_5 resonance

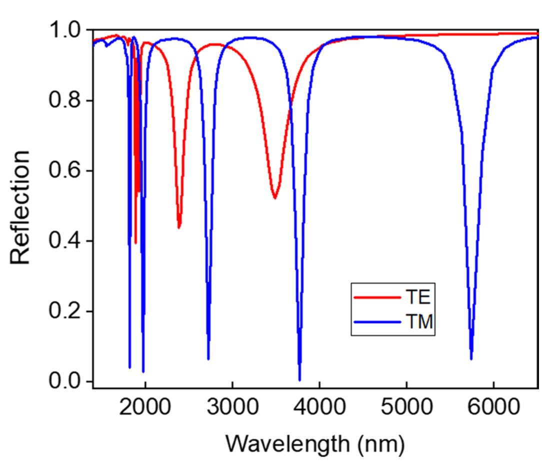

Fig. 5 Polarization dependence of Pi-inverted-Pi antennas. When the antenna was illuminated with TM and TE polarization, deep dips were obtained in TM polarization, while lower peaks were observed in TE polarization

resonances can be controlled. It has also been shown that the MA has high Q factors for each resonance as follows 118.7, 53, 32, 33, and 32, which is beneficial for bio-chemical detections where complex compounds are needed to be identified accurately. Our proposed structure is partially dependent on polarization; therefore, this structure can be used for frequency selectivity, optic absorber and modulators, bio-sensors, active filters, and Raman applications.

Supplementary Information The online version contains supplementary material available at https://doi.org/10.1007/s00339-023-07095-x.

Acknowledgements We would like to thank Karamanoglu Mehmetbey University for its support in the conduct of this study.

Data availability Data will be made available on request.

Declarations

Conflict of interest This work is not financially supported by any agencies and has no personal relationships that could have appeared to influence the work reported in this paper.

References

1. K.S.L. Al-Badri, Revista de Direito, Estadoe Telecomunicacoes **11**(1), 133–144 (2019). https://doi.org/10.26512/lstr.v11i1.22928
2. A. Kabashin, P. Evans, S. Pastkovsky, Nat. Mater. **8**, 867–871 (2009). https://doi.org/10.1038/nmat2546
3. H.T. Nguyen, T.S. Bui, S. Yan, G.A.E. Vandenbosch, P. Lievens, L.D. Vu, E. Janssens, Appl. Phys. Lett. Phys. Lett. (2016). https://doi.org/10.1063/1.4968802
4. J. Kim, K. Han, J.W. Hahn, Sci. Reports. (2017). https://doi.org/10.1038/s41598-017-06749-0

5. B.M. Wells, F. Lotti, M.E. Nasir, A.V. Zayats, V.A. Podolskiy, Opt. Express Express **29**(8), 11562 (2021). https://doi.org/10.1364/OE.418268
6. S.A. Maier, *Plasmonics: Fundamentals and Applications* (Springer US, New York, 2007)
7. Z. Yong, S. Zhang, C. Gong, S. He, Sci. Reports. (2016). https://doi.org/10.1038/srep24063
8. X. Liu, C. Lan, B. Li, Q. Zhao, J. Zhou, Sci. Reports. (2016). https://doi.org/10.1038/srep28906
9. Y. Jia, H. Yin, H. Yao, J. Wang, C. Fan, Result Phys. (2021). https://doi.org/10.1016/j.rinp.2021.104301
10. W. Pan, T. Shen, Y. Ma, Y.Z. Zhang, H. Yang, X. Wang, X. Zhang, Y. Li, L. Yang, Appl. Opt. Opt. **60**(8), 2235 (2021). https://doi.org/10.1364/AO.415461
11. Q. Zhong, T. Wang, X. Jiang, L. Cheng, R. Yan, X. Huang, Opt. Commun. Commun. (2020). https://doi.org/10.1016/j.optcom.2019.124637
12. D. Correas-Serrano, J.S. Gomez-Diaz, J. Perruisseau-Carrier, Alvarez-Melcon, IEEE Trans. Nanotechnol. **13**(6), 1145–1153 (2014). https://doi.org/10.1109/TNANO.2014.2344973
13. D. Wu, N. Fang, C. Sun, X. Zhang, Appl. Phys. Lett. Phys. Lett. **83**(1), 201–203 (2008). https://doi.org/10.1063/1.4826456
14. R.K. Jaiswal, N. Pandit, N.P. Pathak, Plasmonics **14**(6), 1539–1546 (2019). https://doi.org/10.1007/s11468-019-00948-3
15. H. Wang, J. Yang, J. Zhang, J. Huang, W. Wu, D. Chen, G. Xiao, Opt. Lett. Lett. **41**(6), 1233 (2016). https://doi.org/10.1364/OL.41.001233
16. M.R. Pav, N. Granpayeh, S.P. Hosseini, A. Rahimzadegan, Opt. Commun.Commun. **437**, 285–289 (2019). https://doi.org/10.1016/j.optcom.2018.12.071
17. E.D. Palik, S. Diego, L. Boston, N. York, S.T. Toronto, Hand book of Optical Constants of Solids Edited. (1998)
18. S. Khani, M. Danaie, P. Rezaei, Opt. Commun.Commun. **420**, 147–156 (2018). https://doi.org/10.1016/j.optcom.2018.03.047
19. S. Khani, M. Danaie, P. Rezaei, Plasmonics **14**(1), 53–62 (2019). https://doi.org/10.1007/s11468-018-0777-4
20. K. Thirupathaiah, N.P. Pathak, V. Rastogi, IEEE Photon. Technol. Lett. Photon. Technol. Lett. **25**(22), 2217–2220 (2013). https://doi.org/10.1109/LPT.2013.2283880
21. S.M. Ebadi, J. Ortegren, M.S. Bayati, S.B. Ram, IEEE Photon. J. (2020). https://doi.org/10.1109/JPHOT.2020.2974959
22. J. Zhang, X. Yu, J. Dong, W. Yang, S. Liu, C. Shen, J. Duan, X. Deng, Nanomaterials (2021). https://doi.org/10.3390/nano11071824